AJChE 2008, Vol.8 , No.1 , 51 – 60

Investigation on Magnetic Properties of Hematite Superstructures with Controlled Microstructures

Haisheng Qian[a]
Guchang Han[b]
Hong Yang[a]
Guofeng Lin[a]
Rong Xu[*]
[a]*School of Chemical & Biomedical Engineering, Nanyang Technological University, 62 Nanyang Drive, Singapore 637459*
[b]*Data Storage Institute, 5, Engineering Drive I (Off Kent Ridge Crescent, NUS), Singapore 117608*
E-mail: rxu@ntu.edu.sg

Magnetic properties of a series of hematite particles of pseudocubic or pseudoellipsoidal shape consisting of sub-nanoparticles, as well as irregularly shaped hematite agglomerates, were investigated. The microstructures of hematite particles directly obtained from a hydrothermal process were finely controlled with different experimental conditions, such as the type of counter anion, Fe^{3+}/OH^- ratio, surfactant, and aging time. Although samples with different microstructures have a nearly same value of the saturation magnetization, a large variation in the coercivity (H_c) is observed. H_c is found to be closely related to the microcrystal size and its packing density, as well as the formed particle morphologies. The findings obtained in this work contribute to further understanding about the correlation between the microstructural features and the magnetic properties of hematite superstructures. With such fundamental knowledge, it is possible for a systematic search of controlling synthesis parameters which will further lead to the fabrication of hematite particles with optimized magnetic properties for different technological demands.

Keywords: hematite, α-Fe_2O_3, magnetic property, microstructure, superstructure, *and* nanoparticles.

INTRODUCTION

In recent years, hematite (-Fe_2O_3) crystallites of different size, shape and organization have been synthesized by many research groups owing to their potential applications as magnetic recording media, photocatalysts, gas sensors, pigments, anti-corrosive agents and lithium ion batteries (Woo et al. 2003, Cao et al. 2005, Liu et al. 2005, Vayssieres et al. 2005, Tang et al. 2006, Zhu et al. 2007). It is well known that the magnetic properties of hematite, such as the

hysteresis parameters, Morin transition temperature (T_m), etc. are strongly dependent on the microstructure of the hematite particles (Sahu et al. 1997, Rath et al. 1999). In general, low dimensional (0D and 1D) hematite nanoparticles exhibit a weak ferromagnetic nature with a coercive force (H_c) typically in a range of 0.1 to 1 kOe at room temperature (Rath et al. 1999, Jing et al. 2004, Liu et al. 2005, Tang et al. 2006, Zhu et al. 2006). Higher H_c (1-6 kOe) corresponding to ferromagnetism or strong ferromagnetism have been found associated with single-crystalline or polycrystalline -Fe_2O_3 superstructures made of sub-nanoparticle agglomerates (Sahu et al. 1997, Rath et al. 1999, Cao et al. 2005, Zhu et al. 2007). In particular, Mishra and co-workers reported an unusually high H_c of 5.85 kOe pseudocubic hematite particles synthesized by a hydrothermal route (Rath et al. 1999). These monodispersed pseudocubic particles are polycrystalline and consist of large number of highly aggregated sub-nanoparticles. The authors proposed that the large H_c could be contributed by the directional aggregation of sub-nanoparticles inside the cube, which provide a large number of low-angle microcrystal boundaries and dislocations pinning the domain walls. Their findings and together with those from many other groups indicate that the internal microstructure including size, shape and orientation seems to be important in determining the magnetic behavior of hematite particles.

On the other hand, it was observed that hematite nanoparticles with an average diameter of 10 nm obtained from a low-temperature calcination process at 270 °C contains 4.5 wt% of surface water (Lu et al. 2005). The hydration effect is size dependent and becomes less pronounced as the size of nanoparticles increases from 10 to 63 nm. It was noticed that the surface hydration also influences the magnetic behavior of hematite nanoparticles by reducing the interparticle magnetic interactions and the energy barriers for magnetic anisotropy (Predoi et al. 2003). In contrast to the effect of hydration, other researchers reported that the organic residues on the surface of hematite particles resulted from the syntheses in the presence of surfactants are believed to cause the spin pinning and therefore stronger ferromagnetism due to the increase of the magnetic surface anisotropy (Jing et al. 2004a, Jing et al. 2004b, Liu et al. 2005).

In this work, detailed investigations on magnetic properties of a series of hematite particles of pseudo-cubic or pseudoellipsoidal shape consisting of sub-nanoparticles, as well as irregularly shaped hematite agglomerates, have been carried out. The hematite particles were prepared on a large scale by a simple hydrothermal method with different experimental conditions in order to control the microstructures. The results thus obtained provide fundamental knowledge about the correlation between the microstructural features and the magnetic properties of hematite superstructures. In addition, the influences of a few parameters, such as the type of counter anions, surface hydration, and the surfactant molecules, on the microstructural properties are discussed. With such understandings, it is believed that a systematic search of controlling synthesis parameters will further lead to the fabrication of hematite particles with optimized magnetic properties for different technological demands.

EXPERIMENTAL DETAILS

Hematite particles were synthesized by a hydrothermal method. In a typical synthesis, 20 mL of $FeCl_3$ aqueous solution (0.5 M) was added dropwisely into a mixture prepared from 20 mL of NaOH solution (0.5 M) and 3 mL of a nonionic

surfactant, Tween 85, under vigorous stirring at room temperature. The obtained reddish suspension was further treated in an autoclave at 150 °C for 24 h. Finally, the precipitates were collected and washed with large amounts of deionized water and absolute ethanol to remove any impurities. The products were then dried in an oven at 50 °C for 1 d. Other samples were obtained in a similar way with the varied experimental conditions and Table 1 summarizes the synthesis parameters for all the samples.

Table 1. Samples nomenclature and experimental conditions.

sample	counter anion	$[OH^-]$ (M)	Fe^{3+}:OH^- (molar)	Tween 85 (ml)	aging time (h)
A1	Cl^-	0.25	1:0.5	3	24
A2	Cl^-	0.50	1:1	3	8
A3	Cl^-	0.50	1:1	3	24
A4	Cl^-	0.50	1:1	0	24
B	NO_3^-	0.50	1:1	3	24

The crystallographic information of prepared samples was analyzed by powder X-ray diffraction (XRD) method, using a Bruker D8 Advance diffractometer with Cu K radiation (= 1.5406 Å) at a scanning rate of 1 °/min. The average microcrystal sizes, *D*, were calculated from (104) peak using the Scherrer formula (Cullity 1978). The microstructures of all samples were investigated using a JEOL-6700F field emission scanning electron microscope. Chemical bonding information on metal-oxygen, metal-organic groups and hydroxyl were studied with Fourier transform infrared (FTIR, Bio-Rad) using potassium bromide (KBr) pellet technique. Each FTIR spectrum was collected after 40 scans with a resolution of 4 cm^{-1} from 400 to 4000 cm^{-1}. The thermal behavior of samples was analyzed in a TA instrument SDT2960, using thermogravimetric method (TGA). In each run, about 10-11 mg of samples was heated at a rate of 10 °C/min with a flow of air at 100 ml/min. The heating range was from room temperature to 900 °C. Magnetic properties were measured by a Superconducting Quantum Interference Device (SQUID).

RESULTS AND DISCUSSION

Crystal structure and microstructures

The XRD patterns of as-prepared samples are displayed in Figure 1. All diffraction peaks in Figure 1 can be indexed to a hexagonal -Fe_2O_3 phase (JCPDS No: 33-0664). No peaks from impurity phases are detected. It can be seen that all samples prepared by this hydrothermal method are well crystallized and there is only small difference in the diffraction intensities among different samples. The crystal of -Fe_2O_3 has a corundum type structure built on a hexagonal close packed (hcp) array of oxygen in which two thirds of the octahedral sites are occupied by Fe^{3+} ions. The average microcrystal sizes estimated using (104) diffraction peak are shown in Table 2 and they are in the ranges of 28.9 - 43.6 nm. It can be seen that the microcrystal sizes strongly depend on the type of counter anions in the iron precursor. The influence of hematite nanoparticle growth by the impurity anions has been studied previously. It was reported that the anions such as chloride, sulfate and phosphate adsorb on certain crystal planes during the synthesis and the adsorbed anions suppress the crystal growth in the direction perpendicular to that plane (Ozaki et al. 1984, Sugimoto et al. 1993, Sugimoto et al. 1993, Shindo et al. 1994, Ocana et al. 1995, Park et al. 1996, Jia et al. 2005). For example, based on the elemental analysis and internal structure studies of pseudocubic particles, it was proposed that chloride anions adsorbed on {012} planes

Table 2. Microstructure-Dependent Magnetic Properties of Hematite Particles.

sample	shape	particle size (m)	D_{104} (nm)	H_c (Oe)	M_r (emu/g)	T_m (K) Cooling/heating	ΔT_m (K) heating
A1	pseudocubic	0.7~1.1	31.5	2432	0.24	215 / 240.3	30
A2	pseudocubic	0.3~0.6	28.9	4143	0.21	170 / 205	30
A3	pseudocubic	0.4~0.7	30.6	2733	0.21	150 / 185.3	27.3
A4	pseudoellipsoidal	0.5~0.7	34.5	2935	0.25	199.7 / 220.3	13.7
B	irregular	2.0~20.0	43.6	215	0.077	184.7 / 215.3	24.4

retarded the crystal growth in the direction normal to this face (Sugimoto et al. 1993, Park et al. 1996).

However, unlike previous studies, chloride and nitrate anions cannot be observed in the FTIR spectra (not shown) of the hematite samples in this work, indicating that the impurity anions could be removed during the washing step. Some weak adsorption bands at 2929 and 2858 cm^{-1} for samples A1-A3 and B which were synthesized in the presence of Tween 85 were observed. These are due to asymmetric and symmetric C-H stretches of the hydrophobic chain of this surfactant. Similar to our previous observation, it can be suggested that the surface of the hematite particles are capped with certain amount of carboxylated hydrophobic portion of the surfactant after the cleavage of the carbonyl ester group of Tween 85 during the synthesis (Xu et al. 2004). The presence the surface capping organic group affects the morphological properties of the hematite particles, as demonstrated in their SEM images.

The morphologies of the as-prepared hematite solids were examined with the filed emission SEM method. The images shown in Figure 2 indicate that samples A1-A4 prepared from $FeCl_3$ precursor consist of rather uniform particles of pseudocubic (samples A1-A3) and pseudoellipsoidal shapes (sample A4), using the hydrothermal methods in the presence and absence of Tween 85 respectively. It can also be observed in Figure 2 that the particles are all polycrystalline and formed by the aggregates of sub-nanoparticles, in accord with those reported earlier (Sugimoto et al. 1993, Park et al. 1996, Sahu et al. 1997, Rath et al. 1999).

The hematite particles exhibiting pseudocubic shape in these reports were all prepared in the absence of surfactants. As was suggested by Sugioto et al., the specific adsorption of chloride ions and/or chloro ferric complexes to the {012} faces results in the directional aggregation of the sub-nanoparticles which leads to the regularly shaped hematite particles (Sugimoto et al. 1993). Different from the previous results, the hematite particles from the current

synthesis in sample A4 have a pseudoellipsoidal shape, indicating that the morphological properties of hematite particles may be very sensitive to many other experimental conditions besides surfactants, such as temperature, ionic strength, aging time, etc. As summarized in Table 2, the particle sizes of all these samples are in narrow ranges. Among these four samples, sample A1 prepared with a Fe^{3+}/OH^- molar ratio of 2 has the largest size in a range of 0.7-1.1 m. The other three samples prepared with the Fe^{3+}/OH^- molar ratio of 1 are all submicron sized in close ranges between 300-700 nm. The previous investigation has suggested that a decrease in the nominal excess concentration of Fe^{3+} (i.e., a decrease in the Fe^{3+}/OH^- ratio) leads to the enhancement of nucleation and consequently the smaller particle size, during a two-step phase transformation from $Fe(OH)_3$ to -FeOOH and from -FeOOH to -Fe_2O_3 (Sugimoto et al. 1993).

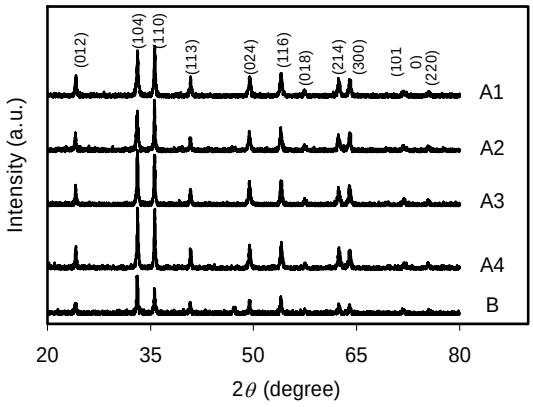

Figure 1. XRD Patterns of Samples A1-A4 and B.

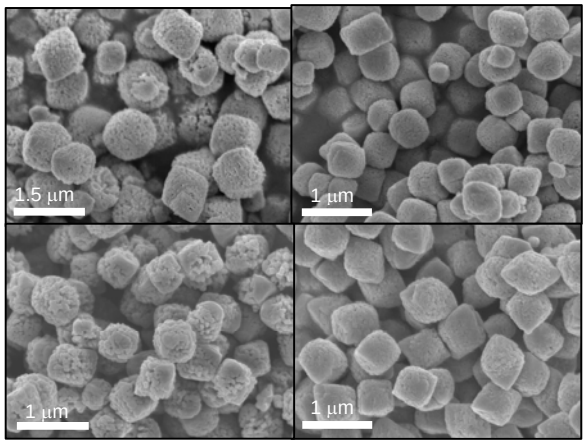

Figure 2. SEM images of hematite samples A1-A4

The difference in the microstructural properties of the particles are analyzed with the high magnification SEM images in Figure 3. Based on the surface morphologies of these particles, several observations can be made. Firstly, the size and size distribution of sub-nanoparticles are affected by the synthesis conditions, although the microcrystal sizes estimated using XRD peaks are very close among the samples. Samples with an aging time of 24 h (A1, A3 and A4) have their sub-nanopartilces sized in 40-60 nm range, while sample A2 aged for 8 h consists of smaller nanoparticles of 30-40 nm. The size comparison between samples A2 and A3 which were prepared with the same conditions except the aging time indicates that the Ostwald ripening process takes place within the pseudocubic particles during the prolonged aging (Ostwald 1897).

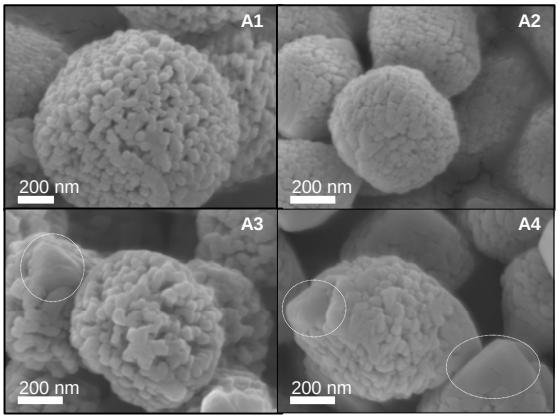

Figure 3. High magnification SEM images of hematite samples A1-A4; the circles in A3 and A4 indicate the smooth and well crystallized areas in these two samples.

Secondly, the packing or the aggregation state of the sub-nanoparticles in these samples varies. A dense packing is observed for samples A2 and A4 which exhibit smoother surface in low magnification SEM images (Figure 2), compared with samples A1 and A3. In the latter two samples, the nanoparticles are loosely aggregated and the interparticle void can be easily observed. Finally, the presence of smooth corners in samples A3 and A4 (circled areas in Figure 3) can be interpreted due to re-crystallization of the aggregated particles in these areas. Since the particles present in the corners have higher surface energy compared with those away from the corners, driven by the energy minimization, interfacial growth between the particles in the corner region takes place, resulting in larger and well crystallized particles. In can be seen that almost all the pseudoellipsoidal particles in sample A4 terminate with two smooth ends. As this sample was prepared in the absence of surfactant, the stronger interaction among the nanoparticles gives rise to such phenomenon. Different from samples A1-A4 with the definite crystal habits, sample B prepared from $Fe(NO_3)_3$ precursor presents irregularly shaped aggregates of loosely packed nanoparticles, as shown in Figure 4.

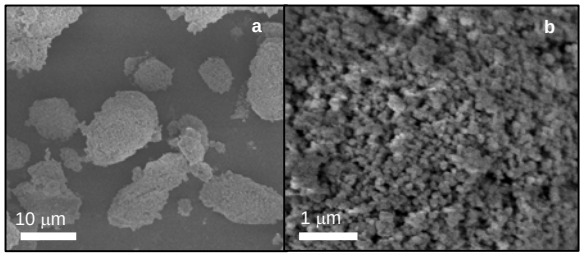

Figure 4. SEM images of sample B: (a) low magnification image, and (b) high magnification image.

It was reported earlier that the magnetic properties of hematite can be significantly modified by surface hydration state (Lu et al. 2005). The hematite samples in this work were all obtained from an aqueous environment and dried at 50 °C without further calcination process. As a result, H_2O and OH^- groups are expected to be present on the surface of our samples. In overall, the total weight loss up to 900 °C for samples A1-A4 in a range of 1.83-2.50% (Figure 5) is substantially lower than those reported in the literature for calcined hematite nanocrystals (Lu et al. 2005). The weight loss before 200 °C is due to the removal of physisorbed water. Sample A2 is slightly more hydrated with a weight loss percentage of 0.82% up to this temperature. It is also known that the hydroxyl groups are present on the surface of metal oxides. The weight loss between 200 to 400 °C could be due to the decomposition of hydroxyl groups and also the decomposition of surface organic groups. In addition, it was suggested that the surface H_2O and OH^- groups exist in energetically different configurations (Jia et al. 2005, Lu et al. 2005)

and therefore, the dehydration and dehydroxylation process takes place in wide range of temperatures, as observed in our studies. The influence of surface H_2O and OH^- groups on the magnetic properties shall not differ significantly among different samples, taking into account of the small amounts of such impurities present on the surface.

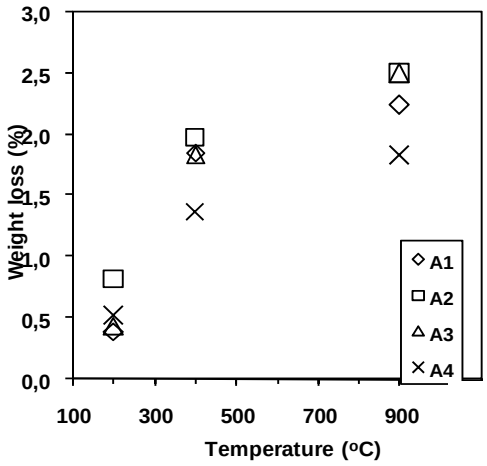

Figure 5. Accumulated weight loss percentage of samples A1-A4 at 200, 400 and 900 °C in flowing air.

Magnetic properties

The ferromagnetism in all samples is demonstrated from the hysteretic magnetization curves obtained by SQUID measurements at 300 K, as shown in Figure 6. All samples show a saturation magnetization of about 0.45 emu/g at 1 Tesla. However, as can be seen from Figure 6, H_c changes from about 4 kOe for sample A2 to 215 Oe for sample B.It is interesting to look into the detailed magnetic characteristics to understand the magnetization process in these samples. As reported previously, the magnetic properties depend on the microstructure of hematite particles (Rath et al. 1999). As can be seen from Figure 4, our samples contain different shape of particles. The particles are in turn composed of many nanocrystals with different packing density. Two microstructural parameters are important to determine the coercivity of the samples. One is the nanocrystal size within the particles. As the magnetostatic coupling among nanocrystals, which is dependent on the boundary condition of the nanocrystals, may be not strong enough to form single domain particles, the magnetization process of particles also involves the magnetization rotation of the individual nanocrystals with different orientations and sizes. A larger H_c c is expected for smaller nanocrystals due to the higher anisotropy energy when they form particles of similar shapes and sizes. This can be seen clearly from the comparison among A1, A2 and A3. On the other hand, the nanocrystals are also magnetically coupled together to form multi-domain particles. The strength of the coupling among the nanocrystals will also affect the magnetization process. The higher H_c obtained for A4 compared to those for A1 and A3 is originated from the stronger coupling of the nanocrystals due to the denser packing and the particle shape because of the higher shape anisotropy in the pseudoellipsoidal particles. Therefore, the H_c of a sample is determined by the interplay of microcrystal size and its packing density, as well as the formed particle morphologies. For sample B, as it has the largest microcrystal size and forms loosely-packed particles, the coercivity is the lowest in all of our samples.

Magnetic properties of α-Fe_2O_3 observed above originate from the so-called Morin transition. Below the transition temperature (T_m), the adjacent spins are antiparallel along the *c*-axis, displaying a bulk antiferromagnetic nature. Above T_m, the magnetic moments are canted in the basal plane, inducing a ferromagnetic behavior.

The bulk T_m is reported to be about 260 K. For compound of small microcrystals, T_m generally decreases as the microcrystal size decreases due to the surface effect (Schroeer et al. 1967). The magnetization (M) of all samples are measured as a function of temperature (T) from 10 to 300 K at various fields.

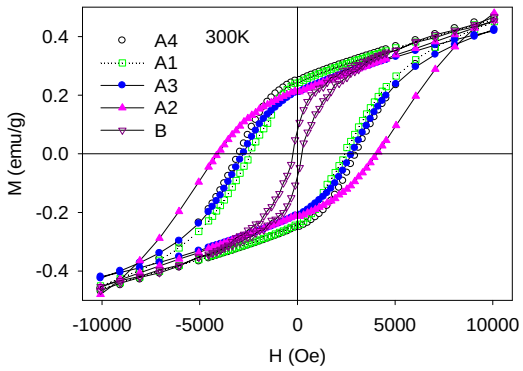

Figure 6. Magnetization curves measured at 300 K for all samples.

To avoid crowding, in Figure 7, only M-T curves measured for sample A3 at two typical fields are shown as an example. To characterize the Morin transition, we define T_m and ΔT_m as the peak temperature and the full width at half maximum of dM/dT curves. It is found that T_m for all samples is much lower than the bulk value. On the contrary to that reported in literatures, we found that T_m is field –dependent for all samples, decreasing monotonically with increasing applied field. Typically, for sample A2, it was found that the temperature shift of the transition can be as high as 25 K when cooling the sample at 5 kOe in comparison with that at 100 Oe. All samples show the shift of the transition to lower temperatures at higher fields in spite of difference of the amplitude. To eliminate the field effect on the transition, T_m and ΔT_m given in Table 2 are measured by cooling at remanent state and heating from 10 K at 0 Oe. It is found that the transition width is much larger than the reported values so far, ranging from 13.7 K for A4 to 30K for A2 when the samples were heated up from 10 K at zero field. The large transition width may be from the broad distribution of the nanocrystal sizes of our samples. It is also noteworthy that the thermal hysteresis appears for all samples, which is in agreement with the Mossbauer measurements reported by Goya et al. (Goya et al. 2005) and can be explained by the surface magnon effect (Chow et al. 1974). From Table 2, it is noted that the broadening of the Morin transition is accompanied by the large thermal hysteresis, which suggests that the thermal hysteresis may be affected by the crystal size distribution.

CONCLUSIONS

In summary, hematite particles of different microstructures have been prepared using a precipitation process under hydrothermal conditions at 150 °C. It was found that the experimental parameters, such as the type of counter anion, Fe^{3+}/OH^- ratio, surfactant, and aging time, affect the size of the sub-nanoparticles as well as their packing density in the overall pseudocubic, pseudoellipsoidal or irregularly shaped particles. It is found that the coercivity is determined by the size of the microcrystals and their packing density, as well as the microstructures of the particles. The results from this work provide deeper understanding about the correlations between the microstructural features and the magnetic properties of hematite particles.

ACKNOWLEDGEMENTS

The authors greatly acknowledge the research funding support from Agency for Science, Technology and Research, Singapore (PSF0521010016).

REFERENCES

Cao, M. H., Liu, T. F., Gao, S., Sun, G. B., Wu, X. L., Hu, C. W., and Wang, Z. L. (2005). "Single-crystal dendritic micro-pines of magnetic alpha- Fe_2O_3: Large-scale synthesis, formation mechanism, and properties," *Angew. Chem. Int. Edit.*, *44*, 4197-4201.

Chow, H., and Keffer, F. (1974). "Soft surface magnons and the first-order magnetic phase transitions in antiferromagnetic hematite," *Phys. Rev. B*, *10*, 243.

Cullity, B. D. (1978). *Elements of X-Ray Diffraction*. Massachusetts, Addison-Wesley.

Goya, G. F., Veith, M., Rapalavicuite, R., Shen, H., and Mathur, S. (2005). "Thermal hysteresis of spin reorientation at Morin transition in alkoxide derived hematite nanoparticles," *Appl. Phys. A Mater. Sci. Process.*, *80*, 1523-1526.

Jia, C. J., Sun, L. D., Yan, Z. G., You, L. P., Luo, F., Han, X. D., Pang, Y. C., Zhang, Z., and Yan, C. H. (2005). "Iron oxide nanotubes - Single- crystalline iron oxide nanotubes," *Angew. Chem. Int. Edit.*, *44*, 4328 – 4333.

Jing, Z. H., and Wu, S. H. (2004a). "Synthesis and characterization of monodisperse hematite nanoparticles modified by surfactants via hydrothermal approach," *Mater. Lett.*, *58*, 3637 – 3640.

Jing, Z. H., Wu, S. H., Zhang, S. M., and Huang, W. P. (2004b). "Hydrothermal fabrication of various morphological alpha-Fe_2O_3 nanoparticles modified by surfactants," *Mater. Res. Bull.*, *39*, 2057 – 2064.

Liu, X. M., Fu, S. Y., Xiao, H. M., and Huang, C. J. (2005). "Preparation and,characterization of shuttle-like alpha- Fe_2O_3 nanoparticles by supermolecular template," *J. Solid State Chem.*, *178*, 2798 – 2803.

Lu, L., Li, L. P., Wang, X. J., and Li, G. S. (2005). "Understanding of the finite size effects on lattice vibrations and electronic transitions of nano alpha- Fe_2O_3," *J. Phys. Chem. B*, *109*, 17151 – 17156.

Ocana, M., Morales, M. P., and Serna, C. J. (1995). "The Growth- Mechanism of Alpha- Fe_2O_3 Ellipsoidal Particles in Solution," *J. Colloid Interface Sci.*, *171*, 85-91.

Ostwald, W. (1897). *Z. Phys. Chem.*, *22*, 289.

Ozaki, M., Kratohvil, S., and Matijevic, E. (1984). "Formation of Monodispersed Spindle-Type Hematite Particles," *J. Colloid Interface Sci.*, *102*, 146-151.

Park, G. S., Shindo, D., Waseda, Y., and Sugimoto, T. (1996). "Internal structure analysis of monodispersed pseudocubic hematite particles by electron microscopy," *J. Colloid Interface Sci.*, *177*, 198-207.

Predoi, D., Kuncser, V., Tronc, E., Nogues, M., Russo, U., Principi, G., and Filoti, G. (2003). "Magnetic relaxation phenomena and inter- particle interactions in nanosized gamma-Fe_2O_3 systems," *J. Phys. Condes. Matter*, *15*, 1797-1811.

Rath, C., Sahu, K. K., Kulkarni, S. D., Anand, S., Date, S. K., Das, R. P., and Mishra, N. C. (1999). "Microstructure-dependent coercivity in monodispersed hematite particles," *Appl. Phys. Lett.*, *75*, 4171-4173.

Sahu, K. K., Rath, C., Mishra, N. C., Anand, S., and Das, R. P. (1997). "Microstructural and magnetic studies on hydrothermally prepared hematite," *J. Colloid Interface Sci.*, *185*, 402-410.

Schroeer, D., and Nininger, R. C. (1967). "Morin Transition in a-Fe_2O_3 microcrystals," *Phys. Rev. Lett.*, *19*, 632-634.

Shindo, D., Park, G. S., Waseda, Y., and Sugimoto, T. (1994). "Internal Structure-Analysis of Monodispersed Peanut-Type Hematite Particles Produced by the Gel-Sol Method," *J. Colloid Interface Sci.*, *168*, 478-484.

Sugimoto, T., Khan, M. M., Muramatsu, A., and Itoh, H. (1993). "Formation Mechanism of Monodisperse Peanut-Type Alpha-Fe_2O_3 Particles from Condensed Ferric Hydroxide Gel," *Colloid Surf. A-Physicochem. Eng. Asp.*, *79*, 233-247.

Sugimoto, T., Muramatsu, A., Sakata, K., and Shindo, D. (1993). "Characterization of Hematite Particles of Different Shapes," *J. Colloid Interface Sci.*, *158*, 420-428.

Tang, B., Wang, G. L., Zhuo, L. H., Ge, J. C., and Cui, L. J. (2006). "Facile route to alpha-FeOOH and alpha-Fe_2O_3 nanorods and magnetic property of alpha- Fe_2O_3 nanorods," *Inorg. Chem.*, *45*, 5196-5200.

Vayssieres, L., Sathe, C., Butorin, S. M., Shuh, D. K., Nordgren, J., and Guo, J. H. (2005). "One-dimensional quantum-confinement effect in alpha- Fe_2O_3 ultrafine nanorod arrays," *Adv. Mater.*, *17*, 2320- 2324.

Woo, K., Lee, H. J., Ahn, J. P., and Park, Y. S. (2003). "Sol-gel mediated synthesis of Fe_2O_3 nanorods," *Adv. Mater.*, *15*, 1761-1765.

Xu, R., and Zeng, H. C. (2004). "Self- generation of tiered surfactant superstructures for one-pot synthesis of Co_3O_4 nanocubes and their closeand non-close-packed organizations," *Langmuir*, *20*, 9780-9790.

Zhu, L. P., Xiao, H. M., and Fu, S. Y. (2007). "Template-free synthesis of monodispersed and single- crystalline cantaloupe-like Fe_2O_3 superstructures," *Cryst. Growth Des.*, *7*, 177-182.

Zhu, L. P., Xiao, H. M., Liu, X. M., and Fu, S. Y. (2006). "Template-free synthesis and characterization of novel 3D urchin-like alpha-Fe_2O_3 superstructures," *J. Mater. Chem.*, *16*, 1794-1797.